Supporting Information for Predicting Adsorption Affinities of Small Molecules on Carbon Nanotubes Using Molecular Dynamics Simulation

Jeffrey Comer*[1,2,3], Ran Chen[1,2], Horacio Poblete[1,2,3], Ariela Vergara-Jaque[1,2,3], and Jim E. Riviere[1,3]

[1]Institute of Computational Comparative Medicine, Kansas State University, Manhattan, Kansas, 66506-5802
[2]Nanotechnology Innovation Center of Kansas State, Kansas State University, Manhattan, Kansas, 66506-5802
[3]Department of Anatomy and Physiology, Kansas State University, Manhattan, Kansas, 66506-5802

Considerations of the Appropriateness of the Theory

The calculation of the adsorption equilibrium constant according to Eq. 4 of the main text may become unreliable when the nanomaterials cannot be represented using models of a roughly flat patch of surface, including materials that form aggregates, as well as those possessing surfaces of high curvature or porosity on the size scale of the adsorbates. Such materials might still be studied by molecular dynamics, but different models and approaches to bridging experiment and simulation would be required.

The assumption of a roughly flat surface appears to be fulfilled for our systems. A comparison of surface areas derived from electron microscopy and the Brunauer–Emmett–Teller method suggests the carbon nanotubes considered here do not have extensive internal cavities relevant for small molecule binding. The number of walls of the multi-wall nanotubes used in the experiments is unknown; however, for the range of outer diameters seen in electron microscopy (8–15 nm) [1], the number of walls likely ranges from 5 to 20, giving specific surface areas [2] from 120 to 340 m^2/g. This range is consistent with that obtained for these nanotubes experimentally by the Brunauer–Emmett–Teller method, 233 m^2/g. Given the uncertainty in the number of walls, however, some binding between the walls rather than on the outer surface cannot be ruled out.

Convergence of the Free Energy Calculations

Below we show that selected free-energy calculations using the adaptive biasing force method show typical convergence behavior as the time of the molecular dynamics simulations is increased. Notably, we find that the correlation between the calculations and experiment increases with simulation time, until plateauing after about 50 ns of simulated time per system.

*E-mail: jeffcomer@ksu.edu

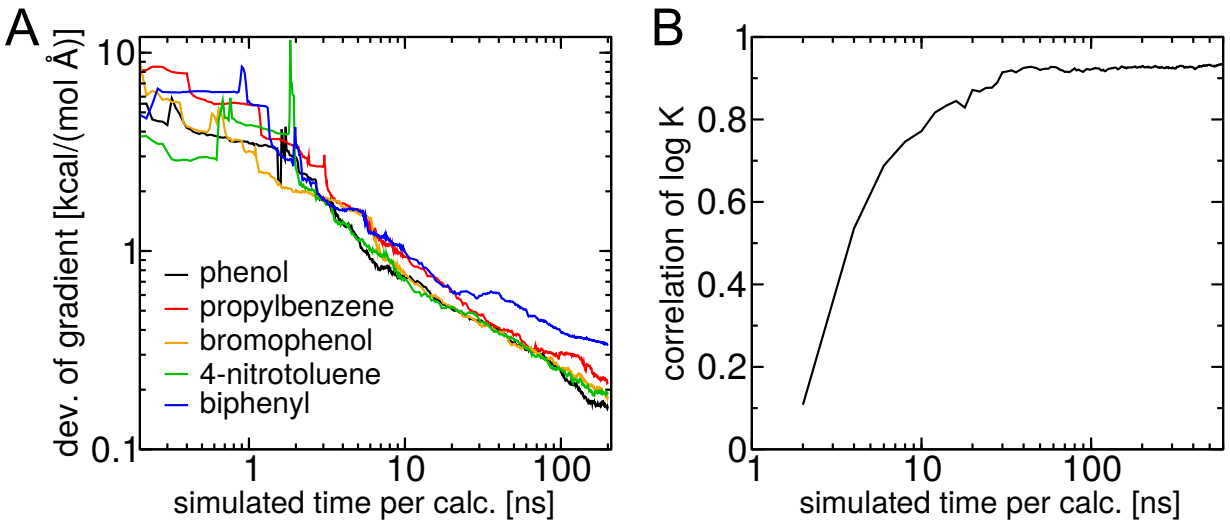

Figure S1: Indicators of convergence. **(A)** Mean-square deviation of the mean force $(-\mathrm{d}w_i^{\mathrm{calc}}(z)/\mathrm{d}z)$ between two independent free-energy calculations as a function of simulated time for the individual calculations. The data is plotted for five exemplary adsorbates. These calculations correspond to the surface model denoted "graph–OH(B)" in the main text. As expected from statistical arguments [3], the deviation between the independent calculations deviation decays as $\sim t^{-1/2}$. **(B)** Convergence of the Pearson correlation coefficient between experimental and simulated values of $\log_{10} K$ for the surface model graph–OH(D) as a function of the length of the free energy calculations. A stable value of 0.93 is obtained only after a few tens of nanoseconds per adsorbate. Note that all data shown in the main text was derived from free-energy calculations comprising > 300 ns of simulated time.

Conformational Sampling

While the figure above demonstrates apparent convergence of the free-energy calculations, to obtain correct free energies, it is necessary to ensure that the sampling is quasi-ergodic, i.e. that all relevant states of the system are adequately sampled in the finite time of the simulations. The adaptive biasing force method guarantees roughly uniform sampling along z, and has the potential to improve sampling along orthogonal coordinates [3]; however, sampling in these coordinates must be verified. Below we show that the minimum length of our simulations (300 ns) was more than adequate to sample a full range of adsorbate positions in the xy plane, as well as a full range of accessible adsorbate orientations. Furthermore, we show that the flexible groups of the polymer conjugated surfaces also sample a wide variety of conformations during the simulations.

The figure below shows biphenyl sampling on three hydroxylated nanotube surfaces with different arrangement. For model graph–OH(B), the hydroxyl groups sterically forbid biphenyl adsorption at some surface positions, permitting adsorption only within nine distinct but identical regions of the model in a range of orientations. On the other hand, biphenyl accesses nearly all parts of the surface not occupied by the hydroxyl groups for graph–OH(C). In contrast to the other models, biphenyl appears to adopt a preferred orientation on model graph–OH(D), i.e. the long axis of the biphenyl molecule tends to align with the hydroxyl pair.

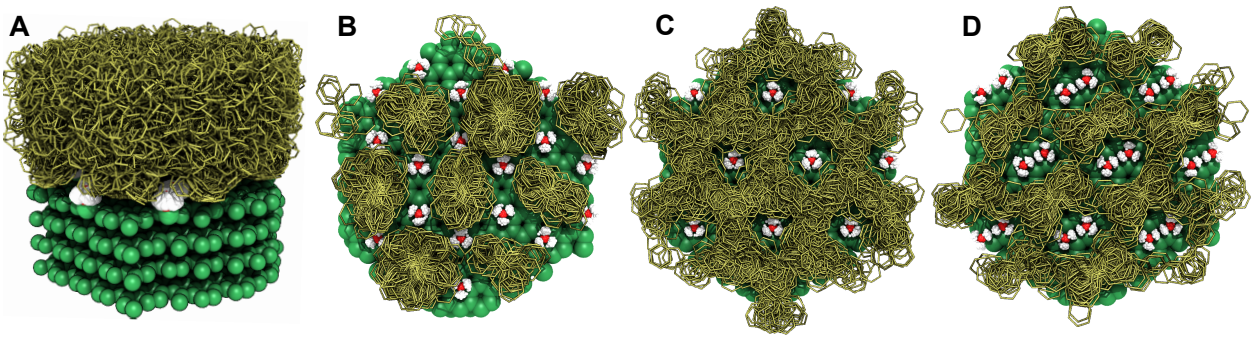

Figure S2: Conformational sampling of biphenyl with hydroxylated nanotube models. (A) Superimposed conformations of a single biphenyl molecule over a 300 ns adaptive biasing force simulation. The 7500 conformations shown were captured at 40 ps intervals, revealing sampling of many different positions and orientations in the window of the free energy calculation ($0.3 \leq z \leq 1.5$ nm). The simulation includes the surface model denoted "graph–OH(D)" in the main text. The biphenyl molecule is represented by yellow sticks, with its hydrogen atoms not shown. The atoms of the hydroxylated nanotube model are shown as spheres with carbon in green, hydrogen in white, and oxygen in red. The conformations of the hydroxyl group over the simulation have also been superimposed. Water is not shown. (B–D) Superimposed conformations biphenyl in contact with the surface for different hydroxylated nanotube models (graph–OH(B), graph–OH(C), graph–OH(D)). Note that periodic boundary conditions and that the system forms a hexagonal tiling of the xy plane. In contrast with panel A, only conformations near the minimum of the free-energy profile are shown, i.e. those for which $0.33 \leq z \leq 4.1$ nm. The hydroxyl groups on the surface populate three favorable ranges of orientation, which is visible in the three-fold arrangement of superimposed hydroxyl hydrogens.

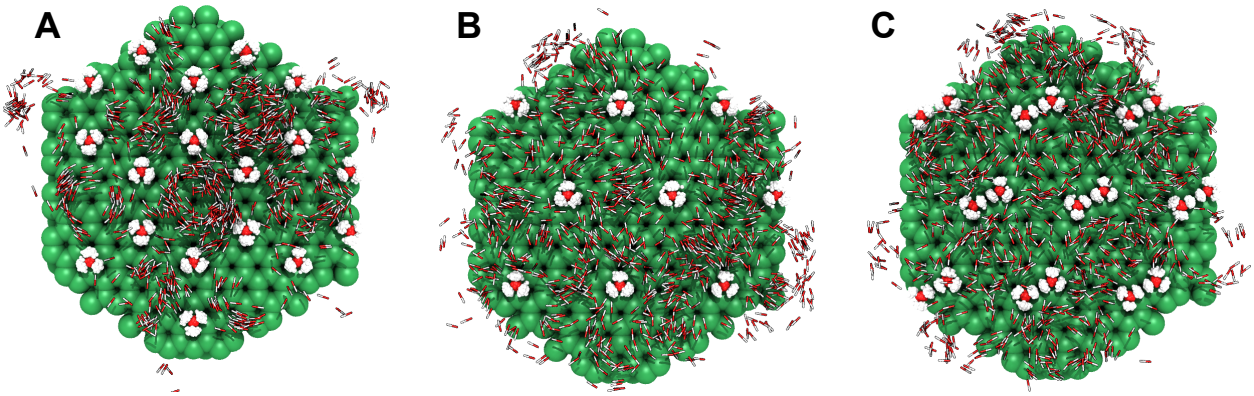

Figure S3: Conformational sampling of m-cresol with hydroxylated nanotube models, focusing on the position and orientation of m-cresol's hydroxyl group. (A–C) Superimposed conformations of the hydroxyl group of m-cresol over a 300 ns adaptive biasing force. The arrangement of hydroxyl groups on the model nanotube surface corresponds to models graph–OH(B), graph–OH(C), and graph–OH(D). Only conformations near the minimum of the free-energy profile are shown, i.e. those for which $0.33 \leq z \leq 4.1$ nm.

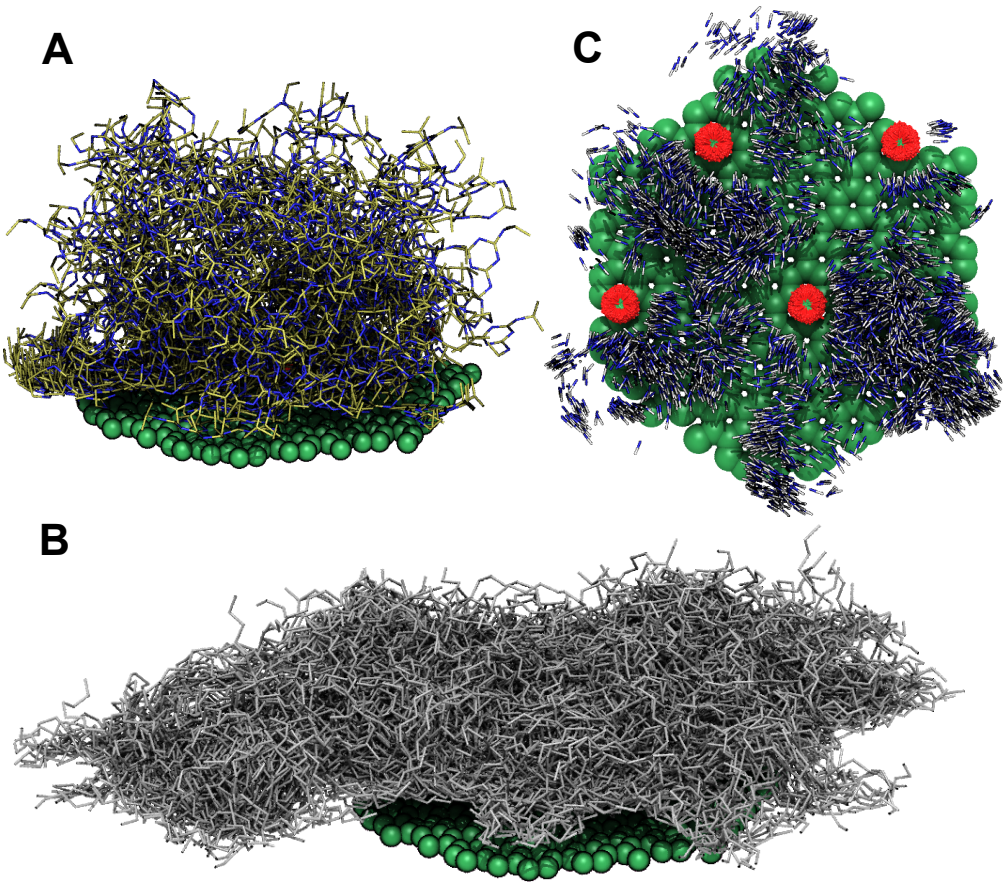

Figure S4: Conformational sampling in adaptive biasing force simulations of atrazine with models of a PEGylated nanotube. (A) Superimposed conformations of atrazine taken at 1 ns intervals over trajectories from multiple walkers and windows (totaling 1.2 μs). Atrazine is represented as sticks, with carbon in yellow, nitrogen in blue, and hydrogen not shown. (B) Superimposed conformations of PEG taken from the same trajectories as in panel A. PEG is shown by gray sticks. (C) Superimposed conformations of the NH groups of atrazine (N in blue, H in white). Only conformations near the minimum of the free-energy profile are shown, i.e. those for which $0.37 \leq z \leq 4.2$ nm. The conformations of the ester linker have also been superimposed (O in red, C in green). For clarity the rest of the PEG molecules are not shown. Hydrogen bonding between the NH group of atrazine and the carbonyl of the ester is apparent.

Robustness of Calculated Free Energy to Different Methodologies

In designing models and simulations to perform free-energy calculations, some seemingly arbitrary decisions must be made. It is important to ensure that these decisions do not have a dramatic effect on the results of the calculations and that the conclusions of the present work are robust to minor changes in methodology. Below we consider the effects of different molecular dynamics simulation parameters and protocols, as well as different choices that might be made in the design of the model and calculation of equilibrium constant. In general, all these effects are small.

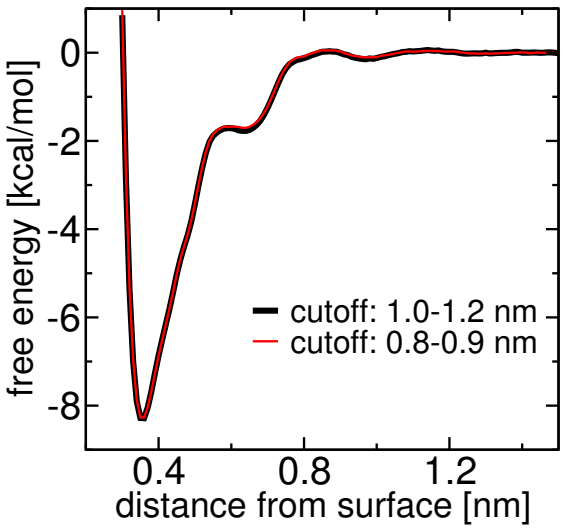

Figure S5: Effect of different force truncation schemes in the molecular dynamics simulations on calculated free energy. In molecular dynamics simulations, van der Waals forces are often smoothly reduced to zero at a particular distance to avoid the computational cost associated with computing forces between all pairs of atoms, which rises quadratically with the number of atoms. Using a relatively low value of this truncation distance (0.9 nm) improves performance, which increases amount of sampling that can be feasibly done for each system. However, unphysical truncation of the van der Waals force can lead to systematic errors [4]; Thus, there is a trade-off between using the most physically accurate model, which reduces systematic error, and obtaining better sampling, which reduces statistical error. Therefore, we sought to determine whether our choice of the truncation distance led to any clear systematic change in the free energy. Plotted are the potentials of mean force as a function of the distance between a biphenyl molecule and a multi-wall carbon nanotube surface model, similar to that shown in Fig. 1 of the main text. The black curve shows the result of the free energy calculation with van der Waals forces smoothly truncated from 1.0 to 1.2 nm (`switchDist 10` and `cutoff 12` in the NAMD 2.10 configuration file), while the red curve shows the result with a 0.8 to 0.9 nm cutoff (`switchDist 8` and `cutoff 9`). Each simulation comprised 420 ns of simulated time. The potentials of mean force were essentially identical (indistinguishable considering statistical error). The shorter cutoff distance leads to substantially improved performance (50–100%) and was therefore used in all production simulations.

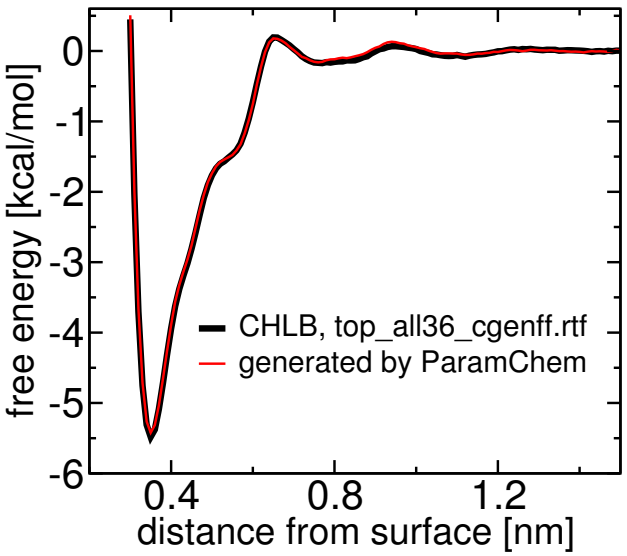

Figure S6: Effect of different CHARMM general force field (CGenFF) models on calculated free energy. In some cases, the partial atomic charges automatically generated by the CGenFF program differed from a model compound defined by hand in the CGenFF force field. In most cases, these differences were only a few thousandths of the elementary charge. The largest differences ($0.016e$) were seen for chlorobenzene. For this reason, here we compare the "official" chlorobenzene model to the automatically generated version. Plotted are the potentials of mean force as a function of the distance between a chlorobenzene molecule and a multi-wall carbon nanotube surface model, similar to that shown in Fig. 1 of the main text. The black and red lines show the results for the "official" model of chlorobenzene included with the CGenFF force field distribution [5] and that produced automatically by the CGenFF program [6, 7]. The difference between the two potentials of mean force is quite small, leading to $\log_{10} K^{\mathrm{calc}}_{\mathrm{ClBn}}$ values, 1.97 and 1.93, that are essentially identical for the purposes of the present work. All data shown in the main text uses the chlorobenzene model produced automatically by the CGenFF program. For each model, the free-energy calculation comprised 480 ns of simulated time. The difference in the free energies between the two models ($\sim$0.1 kcal/mol) was irrelevant to the present work, having a negligible effect on the comparisons between experiment and calculation. All values presented in the main text were performed with the automatically generated atomic partial charges.

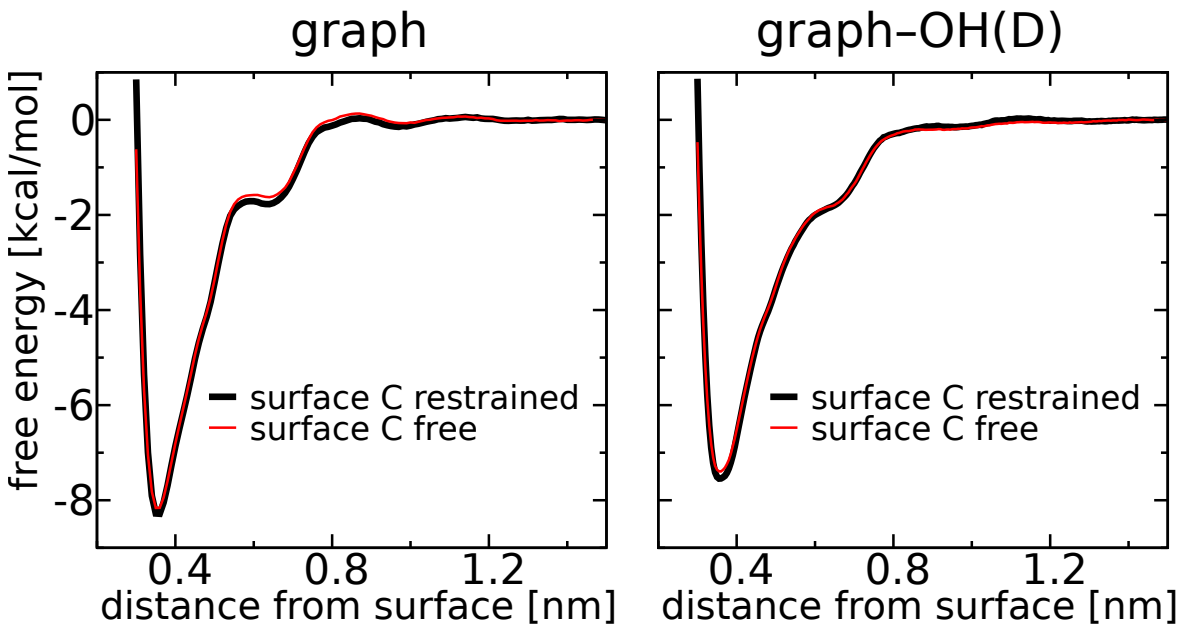

Figure S7: Effect of applying harmonic restraints to surface carbon atoms on calculated free energy. For all data described in the main text, the sp^2 carbon atoms of the graphene sheet were restrained to their ideal positions using weak harmonic restraints. The restraint potential for atom i was given by

$$E_i = K^{\text{rest}} |\mathbf{r}_i - \mathbf{R}_i|^2 \tag{1}$$

where $K^{\text{rest}} = 1.0$ kcal/(mol Å^2) and $\mathbf{r}_i$ and $\mathbf{R}_i$ were the current and ideal positions for atom i. To determine what effect these restraints might have, we performed additional free-energy calculations for biphenyl on two different surfaces with restraints on the upper layer of graphene removed. In these calculations, the upper layer of graphene slid freely over the lower layers as it underwent lateral diffusion. Plotted are the potentials of mean force as a function of the distance between a biphenyl molecule and the nanotube surface for the naked carbon nanotube model (A) and the hydroxylated carbon nanotube model denoted "graph–OH(D)" in the main text (B). The restraints may reduce the deformability of the graphene layer leading to the slight differences seen in the plot. Notably, the free energy minima are less favorable by 0.1–0.15 kcal/mol, which should not effect the conclusions of the present work, but may be statistically significant. Given that the restraints used in the majority of simulations were unnecessary and may perhaps yield small unphysical effects, we do not recommend their use. If restraints are desired for convenience of analysis, a better solution would to apply restraints only to the lower layers of the graphene (as we have done here), or restrain the center of mass of the graphene layer rather than individual atoms.

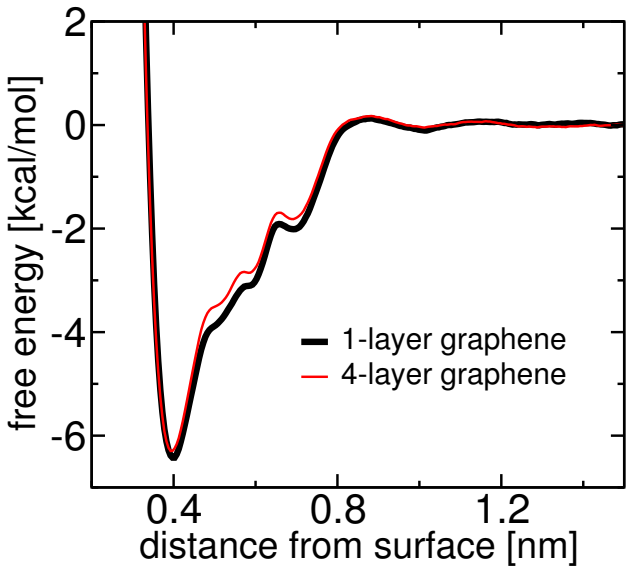

Figure S8: Comparison of adsorption for single- and multiple-layer graphene. Plotted are the potentials of mean force as the function of the distance between the center of mass of atrazine and a graphene surface. The black curve is derived from a model containing only a single layer of graphene solvated above and below, while model from which the red curve is derived contains four layers of graphene in a graphite arrangement. The latter model is similar to that in Fig. 1 of the main text. Although the difference between the two systems is statistically significant, it is quite small. Thus, the internal structure of the nanotubes may be of little relevance in studies of small molecule adsorption to their surfaces.

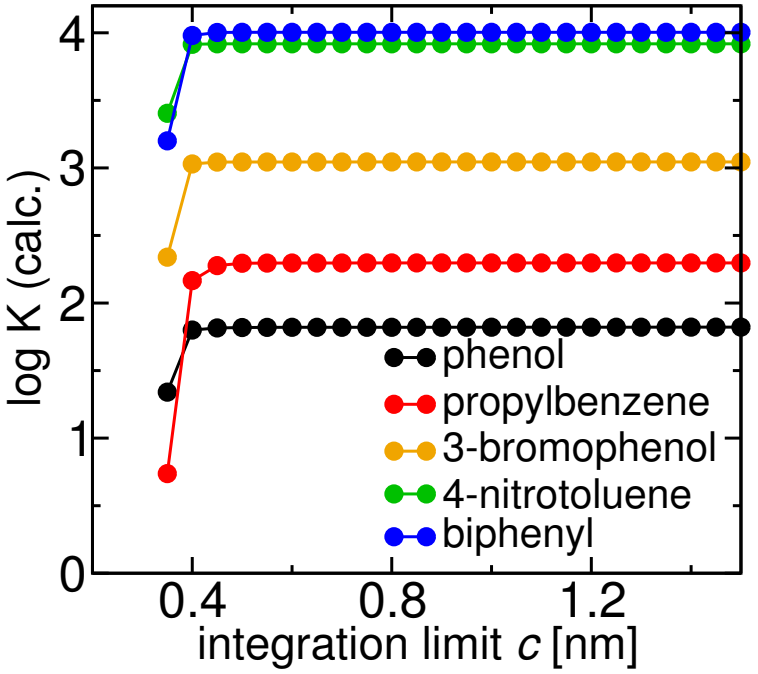

Figure S9: Effect of the choice of the upper limit of the integral in Eq. 4 of the main text. Plotted are the $\log_{10} K^{\mathrm{calc}}$ values for adsorption of exemplary small aromatics onto a model of naked carbon nanotubes similar to those shown in Fig. 1. Due the the exponential contribution of $w_i^{\mathrm{calc}}(z)$ to the

integral, the value of $\log_{10} K^{\mathrm{calc}}$ is determined almost exclusively by the $w_i^{\mathrm{calc}}(z)$ values near the global minimum of the $w_i^{\mathrm{calc}}(z)$ ($0.35 < z < 0.37$ nm). Thus, the results are effectively identical for any reasonable choice of c.

Free Energy Perturbation. To further verify the results of adaptive biasing force, we performed free energy perturbation calculations for three exemplary systems. The equilibrated systems, including biphenyl (bPh), *m*-cresol (mCr) and toluene (T) complexed with a surface of multi-wall carbon nanotubes, were used as a starting point to determine the binding free energy of each complex. The free energy differences were estimated employing the free energy perturbation (FEP) method [8], wherein each molecule was gradually annihilated from bulk solution as it gradually appeared on the graphenic surface. For each FEP calculation, 160 intermediate states ($\Delta\lambda = 0.00625$) were considered in the forward and backward directions [9], involving for each state 0.5 ns of equilibration followed by 0.5 ns of data collection. For each of the three molecules, a simulation time of 320 ns was invested. Weak harmonic restraints (force constant 1 kcal/(mol Å^2)) were used to keep the molecule near the free energy minimum on the surface (z=0.35 nm), whereas the molecule in bulk solution was kept at a distance from the surface, $1.45 < z < 1.55$ nm, using a flat bottom harmonic potential. All restraints were applied utilizing the collective variable module [10] available in the NAMD 2.9 [11]. The ParseFEP plugin [12] of VMD 1.9.2 [13] was employed to determine the SOS[12] and BAR[14] estimators alongside with its statistical error by combining forward and backward transformations. The table below provides a comparison of the FEP results with those of adaptive biasing force. The FEP and adaptive biasing force values agree to within the statistical error or nearly so.

Compound	Forward	Backward	BAR	SOS	ABF
toluene	-5.06	4.97	-4.89 ± 0.04	-5.03 ± 0.04	-5.05
m-cresol	-6.40	6.54	-6.32 ± 0.04	-6.49 ± 0.04	-6.38
biphenyl	-7.85	8.14	-7.82 ± 0.05	-8.06 ± 0.06	-8.20

Table S1: A comparison of change in free energy upon adsorption calculated by free energy perturbation and the minimum of the potential of mean force calculated by adaptive biasing force (ABF). The result of the forward and backward calculations are shown, along with the BAR and SOS estimators. All energies are in kcal/mol.

Adsorption Kinetics

The procedure to calculate the diffusivity has been detailed elsewhere [3, 15]. Briefly, the dynamics of the adsorbates is assumed to obey overdamped Brownian dynamics with the following discretized form

$$z_{t+\Delta t} - z_t = \beta D(z_t)[f^{\mathrm{sys}}(z_t) + f^{\mathrm{bias}}(t)]\Delta t + \nabla D(z_t)\Delta t + (2D(z_t)\Delta t)^{1/2} g_t, \tag{2}$$

where z_t is the distance of the adsorbate from the surface at time t, $D(z)$ and $f^{\mathrm{sys}}(z_t) = -\nabla w(z)$ are the diffusivity and system force along coordinate z, f^{bias} is the adaptive biasing force, and g_t is a random variable with a standard normal distribution. The likelihood of the simulated trajectory,

given trial forms of $D(z)$ and $f^{\mathrm{sys}}(z)$, is calculated as

$$P[z(t) \,|\, f^{\mathrm{sys}}(z), D(z)] = \prod_{\alpha} \frac{1}{\sqrt{4\pi D(z_{t_\alpha})\Delta t}} \exp\left(-\frac{\left\{ z_{t_\alpha+\Delta t} - z_{t_\alpha} - \beta D(z_{t_\alpha})[f^{\mathrm{sys}}(z_{t_\alpha}) + f^{\mathrm{bias}}(t_\alpha)]\Delta t - \nabla D(z_{t_\alpha})\Delta t \right\}^2}{4D(z_{t_\alpha})\Delta t} \right). \tag{3}$$

Using Bayes' theorem, we calculate the probability of the parameters given the trajectory from the likelihood above

$$P[f^{\mathrm{sys}}(z), D(z) \,|\, z(t)] = p_{\mathrm{prior}}(f^{\mathrm{sys}}(z), D(z)) \times P[z(t) \,|\, f^{\mathrm{sys}}(z), D(z)]. \tag{4}$$

The best estimate of the diffusivity is found by maximizing this probability by a Monte Carlo search of $f^{\mathrm{sys}}(z)$ and $D(z)$ functions. For the figure below, we chose $\Delta t = 8$ ps and $p_{\mathrm{prior}} = p_{\mathrm{scale}} p_{\mathrm{smooth}}$, where $p_{\mathrm{scale}} = \prod_j 1/D(z_j)$ is the scale-invariance prior [16] and $p_{\mathrm{smooth}} = \prod_j \exp\left\{ -[D(z_{j+1}) - D(z_j)]^2 / (2\epsilon^2) \right\}$ is a prior that assumes smoothness. The latter used the value $\epsilon = 20$ nm^2/ns, which, at a grid spacing of 0.01 nm, only weakly imposes smoothness. After obtaining converged $D(z)$ and $f^{\mathrm{sys}}(z)$ functions, we calculated the mean first-passage time [17] by

$$\tau_{a\to b} = \int_a^b \mathrm{d}\zeta \, \exp[\beta w(z)]/D(z) \times \int_a^z \mathrm{d}z' \, \exp[-\beta w(z')] \tag{5}$$

where a is the position of the free energy minimum ($z = 0.35$ nm) and b is the point to which the travel time is desired. The results of these calculations are shown in the figure below.

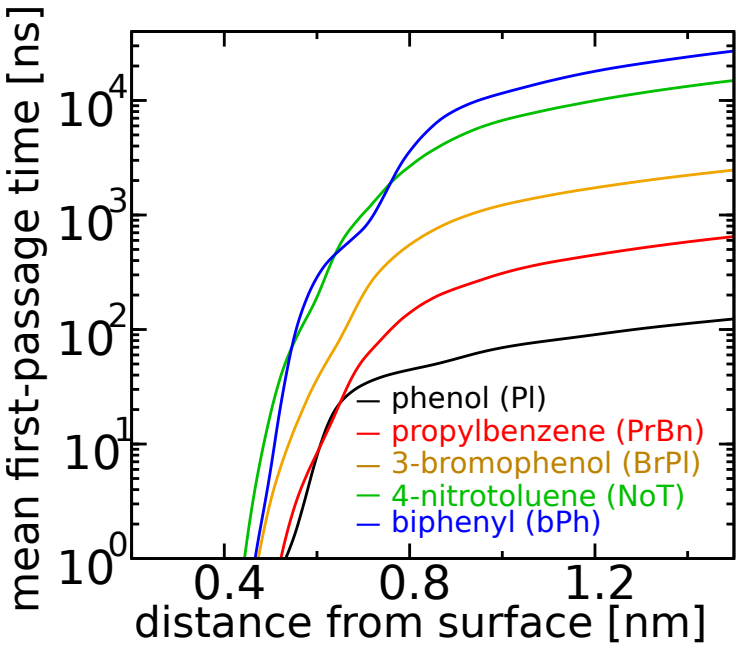

Figure S10: Kinetics of surface desorption for three exemplary adsorbates. Plotted is the mean first passage time from the free-energy minimum (near $z = 0.35$ nm) to the distance on the horizontal axis.

Grand-Canonical Monte Carlo/Brownian Dynamics

Similar to previous work [18], in the grand-canonical Monte Carlo/Brownian dynamics simulations (GCMC/BD), each molecule was represented as a spherically symmetric particle. Brownian dynamics [19] were performed in 3 dimensions by updating molecule positions according to the rule

$$\mathbf{r}_i(t+\Delta t) = \mathbf{r}_i(t) - \beta D \Delta t \, \nabla_i W(\mathbf{r}_1 \dots \mathbf{r}_N) + \sqrt{2D\Delta t}\, \mathbf{R}_t, \tag{6}$$

where $D = 1.3$ nm^2/ns was the diffusion constant, $\Delta t = 10$ fs was the timestep, and $\mathbf{R}_t$ were 3-vectors of Gaussian random numbers (of zero mean and unity variance). The value of the diffusion constant was mostly irrelevant because we did not consider kinetics. The multi-particle potential of mean force consisted of an external term due to the surface (derived from the free-energy calculations described above) and an effective interaction energy between pairs of molecules: $W(\mathbf{r}_1 \dots \mathbf{r}_N) = \sum_i w_i(z_i) + \sum_{i,j} V_{ij}(\mathbf{r}_i, \mathbf{r}_j)$. The intermolecular interaction had the Lennard-Jones form:

$$V_{ij}(\mathbf{r}_i, \mathbf{r}_j) = 4\epsilon \left(\frac{\sigma_{ij}^{12}}{|\mathbf{r}_i - \mathbf{r}_j|^{12}} - \frac{\sigma_{ij}^{6}}{|\mathbf{r}_i - \mathbf{r}_j|^{6}} \right). \tag{7}$$

This interaction was smoothly truncated from 0.13 to 0.15 nm using a standard switching function [20]. The interaction distance, σ_{ij}, was chosen to reproduce the area of the graphene surface occluded by the molecule in explicit-solvent simulation, as follows. We selected frames from the trajectories where molecule i was adsorbed ($0.335 < z < 0.390$ nm) and computed the average number of water molecules in the adsorbed layer ($0.3 < z < 0.5$ nm) over these frames, $\langle N_i^{\mathrm{w}} \rangle$. The existence of this adsorbed water layer is evident from the black curve in Fig. 4B of the main text. The area of the surface occupied by the molecule i was estimated by

$$a_i = \left(1 - \frac{\langle N_i^{\mathrm{w}} \rangle}{\langle N_0^{\mathrm{w}} \rangle} \right) A, \tag{8}$$

where $\langle N_0^{\mathrm{w}} \rangle = 76.54$ was the average number of adsorbed water molecules in the absence of solutes and $A = 7.522$ nm^2 was area of the graphene–water interface. The interaction distance was then calculated as $\sigma_i = 2\sqrt{a_i/\pi}$ and interactions between unlike molecules by $\sigma_{ij} = (\sigma_i + \sigma_j)/2$. In all cases, $\epsilon_{ij} = 1.6$ kcal/mol based on Fig. S11. At intervals of 100 steps, grand canonical Monte Carlo moves to create and delete molecules (chosen with equal probability) were attempted 10 times for each type of molecule. Creation and deletion moves were accepted with the probabilities

$$P_{\mathrm{cre}} = \frac{n_\alpha V_0 / (N_\alpha + 1) \mathrm{e}^{-\beta \Delta W}}{1 + n_\alpha V_0 / (N_\alpha + 1) \mathrm{e}^{-\beta \Delta W}}, \tag{9}$$

$$P_{\mathrm{del}} = \frac{1}{1 + n_\alpha V_0 / N_\alpha \mathrm{e}^{+\beta \Delta W}}, \tag{10}$$

where $n_\alpha = c_i^{\mathrm{eq}} / M_i$ was desired number of density of molecules in bulk solution, V_0 was the volume of the simulation system and ΔW was the change in multi-particle potential of mean force due to the trial move. The excess chemical potential was not included since the bulk densities were so low that the solution was essentially ideal (typically only one or two molecules were present in the bulk region of the simulation box). The simulation system was a cube with a 80 nm side length, periodic in the x and y directions and with reflecting boundaries on the z-faces. At the bottom face of the cube, the function $w_i(z)$ represented the interaction with the surface and was zero elsewhere. Molecule creation occurred with uniform probability over the entire box, including at the surface, while molecules to be deleted were selected at random from the entire box. The simulation began with no molecules in the box and was run for 5 μs to obtain steady equilibrium populations of molecules on the surface.

GCMC/BD Results. We represent each molecule by a single particle, which moves randomly according to the Brownian dynamics equation of motion and interacts with the surface according to the $w_i^{\mathrm{calc}}(z)$ for that type of molecule. Through grand-canonical Monte Carlo, we attempt to create and delete molecules randomly throughout the entire system, which allows an equilibrium to be relatively rapidly established between the surface where the adsorbate density is high and the fixed concentration in bulk solution. With no interactions between the molecules, the (GCMC/BD) procedure yields the expected mean number density, $n_i(z) = n_i^{\mathrm{bulk}} \exp\left[-\beta w_i^{\mathrm{calc}}(z)\right]$, where n_i^{bulk} is the fixed number density of molecules in bulk solution. However, the effect of surface loading can be estimated by including appropriate intermolecular interactions. We use a Lennard-Jones form for these interactions as described above. The bulk number density of each molecule is set to the equilibrium value in the experiment, $n_i^{\mathrm{bulk}} = c_i^{\mathrm{eq}}/M_i$. The adsorption equilibrium constant is then calculated by

$$K_i^{\mathrm{calc}} = \frac{A_{\mathrm{NP}}}{M_{\mathrm{NP}}} \int_0^c \mathrm{d}z\, n_i(z)/n_i^{\mathrm{bulk}}, \tag{11}$$

where $n_i(z)$ is the number density of adsorbate i. Applying this equation to the GCMC/BD trajectories yields only changes in the $\log_{10} K_i^{\mathrm{calc}}$ values (averaging ~ -0.009) relative to those calculated by Eq. 3 in the main text, which are negligible for this work. Thus, intermolecular interactions are probably not sufficient to explain the discrepancies between simulation and experiment, and are neglected for the rest of this paper.

Additional Free-Energy Calculations

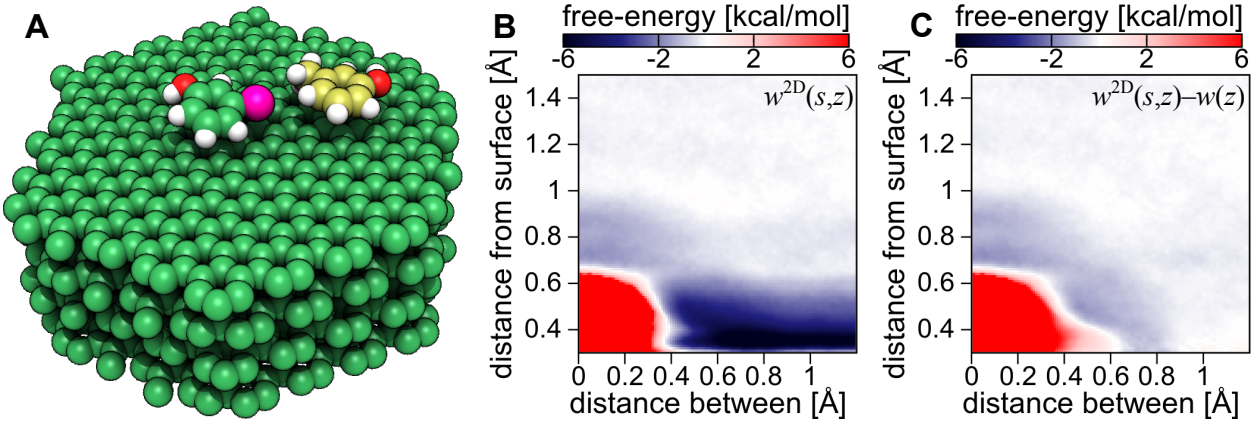

Figure S11: Adsorption to a surface already occupied by another molecule. (A) Snapshot from a free-energy calculation of *m*-cresol (mCr) adsorption to a model naked carbon nanotube surface occupied by a molecule of 3-chlorophenol (ClPl). (B) The two-dimensional free-energy landscape, $w^{2D}(z, s)$. As in the other calculations in this work, the first variable, z, was the projection along the z axis of the vector from the center of mass of the first layer of graphene to the center of mass of the mCr molecule. The second variable, $s = \sqrt{(x - x_0)^2 + (y - y_0)^2}$ was the distance between the mCr and ClPl molecules projected into the xy plane. The geometric term in the potential of mean force, $-k_{\mathrm{B}}T \ln(2\pi s)$, was been subtracted (using the `hideJacobian` option of the Colvars module [10]). (C) The free-energy landscape in panel B after subtracting the surface interaction $w_{\mathrm{mCr}}^{\mathrm{calc}}(z)$, determined from a previous one-dimensional free-energy calculation. A region of attraction surrounding the adsorbed molecule (≈ -1.6 kcal/mol) is evident.

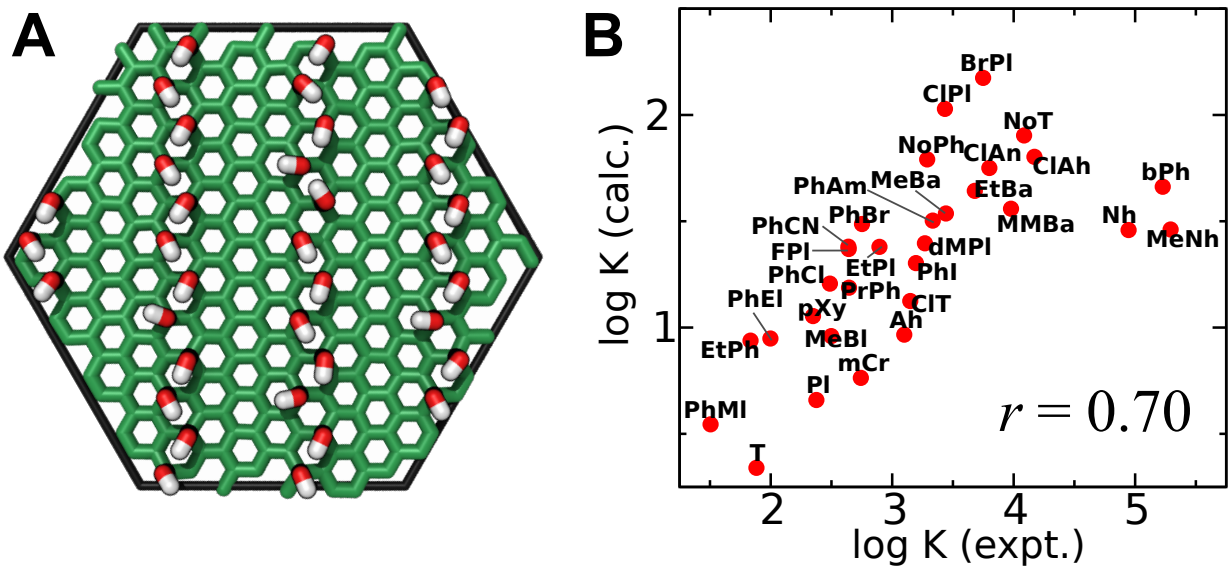

Figure S12: Model hydroxylated carbon nanotube with an alternate arrangement of OH groups. (A) Arrangement of 36 OH groups on a graphene surface at a density of 4.8 groups/nm^2. (B) Comparison between the logarithm of the adsorption equilibrium constant determined from experiment and that calculated from simulations for the arrangement shown in panel A.

References

1. Xia XR, Monteiro-Riviere NA, Mathur S, Song X, Xiao L, Oldenberg SJ, Fadeel B, Riviere JE (2011) Mapping the surface adsorption forces of nanomaterials in biological systems. *ACS Nano* 5(11):9074–9081.

2. Peigney A, Laurent C, Flahaut E, Bacsa R, Rousset A (2001) Specific surface area of carbon nanotubes and bundles of carbon nanotubes. *Carbon* 39(4):507–514.

3. Comer J, Gumbart JC, Hénin J, Lelièvre T, Pohorille A, Chipot C (2014) The adaptive biasing force method. everything you always wanted to know, but were afraid to ask. *J Phys Chem B* 119(3):1129–1151. doi:10.1021/jp506633n.

4. Huang K, García AE (2014) Effects of truncating van der Waals interactions in lipid bilayer simulations. *J Chem Phys* 141(10):105101.

5. Vanommeslaeghe K, Hatcher E, Acharya C, Kundu S, Zhong S, Shim J, Darian E, Guvench O, Lopes P, Vorobyov I, MacKerell AD (2010) CHARMM general force field: A force field for drug-like molecules compatible with the CHARMM all-atom additive biological force fields. *J Comput Chem* 31(4):671–690.

6. Vanommeslaeghe K, MacKerell Jr AD (2012) Automation of the CHARMM general force field (CGenFF) I: Bond perception and atom typing. *J Chem Inf Model* 52(12):3144–3154.

7. Vanommeslaeghe K, Raman EP, MacKerell Jr AD (2012) Automation of the CHARMM general force field (CGenFF) II: Assignment of bonded parameters and partial atomic charges. *J Chem Inf Model* 52(12):3155–3168.

8. Zwanzig RW (1954) High-temperature equation of state by a perturbation method. I. Nonpolar gases. *J Chem Phys* 22(8):1420–1426.

9. Pohorille A, Jarzynski C, Chipot C (2010) Good practices in free-energy calculations. *J Phys Chem B* 114:10235–10253.

10. Fiorin G, Klein ML, Hénin J (2013) Using collective variables to drive molecular dynamics simulations. *Mol Phys* 111(22-23):3345–3362.

11. Phillips JC, Braun R, Wang W, Gumbart J, Tajkhorshid E, Villa E, Chipot C, Skeel RD, Kale L, Schulten K (2005) Scalable molecular dynamics with NAMD. *J Comput Chem* 26:1781–1802.

12. Liu P, Dehez F, Cai W, Chipot C (2012) A toolkit for the analysis of free-energy perturbation calculations. *J Chem Theory Comput* 8(8):2606–2616.

13. Humphrey W, Dalke A, Schulten K (1996) VMD – Visual Molecular Dynamics. *J Mol Graphics* 14:33–38.

14. Bennett CH (1976) Efficient estimation of free energy differences from Monte Carlo data. *J Chem Phys* 22(2):245–268.

15. Comer JR, Chipot CJ, Gonzalez-Nilo FD (2013) Calculating position-dependent diffusivity in biased molecular dynamics simulations. *J Chem Theory Comput* 9(2):876–882. doi:10.1021/ct300867e.

16. Best R, Hummer G (2011) Diffusion models of protein folding. *Phys Chem Chem Phys* 13(38):16902–16911.

17. Schulten K, Schulten Z, Szabo A (1981) Dynamics of reactions involving diffusive barrier crossing. *J Chem Phys* 74:4426–4432.

18. Carr R, Comer J, Ginsberg M, Aksimentiev A (2011) Atoms-to-microns model for small solute transport through sticky nanochannels. *Lab Chip* 11:3766–3773. doi:10.1039/C1LC20697D.

19. Ermak D, McCammon J (1978) Brownian dynamics with hydrodynamic interactions. *J Chem Phys* 69:1352.

20. Dubbeldam D, Torres-Knoop A, Walton KS (2013) On the inner workings of Monte Carlo codes. *Mol Sim* 39(14-15):1253–1292.